CrystEngComm

Accepted Manuscript

ROYAL SOCIETY OF CHEMISTRY

www.rsc.org/crystengcomm

Cite this: DOI: 10.1039/c0xx00000x

www.rsc.org/xxxxxx

ARTICLE TYPE

Hydrothermal synthesis and formation mechanism of single-crystalline perovskite $BiFeO_3$ microplates with dominant (012) facets

Xin Yang, Gang Xu,* Zhaohui Ren, Xiao Wei, Chunying Chao, Siyu Gong, Ge Shen and Gaorong Han*

Received (in XXX, XXX) Xth XXXXXXXXX 20XX, Accepted Xth XXXXXXXXX 20XX

DOI: 10.1039/b000000x

A facile hydrothermal method was developed to prepare single-crystal $BiFeO_3$ (BFO) microplates, where raw material ($C_6H_{10}BiNO_8$) was used both as a reactant and a surface modifier. The as-synthesised BFO microplates were dominated by (012) facets with the lateral length of 8 μm and thickness of 510-550 μm. The results of XRD, SEM, TEM, HRTEM and FT-IR indicate that adsorption behaviour of the organic ligands could play key role in the formation of the BFO microplates. Moreover, the dielectric constant of the BFO-PVDF film is much higher than pure BFO at room temperature. The special chosen of raw materials ($C_6H_{10}BiNO_8$) and the proposed formation mechanism of BFO microplates could be extended to tailor the crystal growth of 2D structures of other perovskite oxides.

Introduction

Perovskite ferroelectric oxides nanostructures have become the focus of many studies because of their fascinating properties, such as ferroelectricity, dielectricity and piezoelectricity, and their potential applications in novel devices.[1] As a result, many perovskite ferroelectric oxide nanostructures, such as nanoparticles, nanorods, nanowires and nanotubes, have been obtained by using melting salt method, hydrothermal route and etc. However, the reports mostly focus on the zero-dimensional (0D) and one-dimensional (1D) nanostructures scarcely on the two-dimensional nanostructures up to now[2-5].

Over the past years, two-dimensional (2D) nanostructures, such as nanosheets, nanoplates and nanoflakes, are also highly attracted extensive attentions because of their potential performances. Recent theoretical research predicts that ferroelectric nanodiscs could even favour an ultimate NFERAM density of 60×10^{12} bits per square inch as well as a new toroid moment[6]. To date, different approaches, such as focused ion beam (FIB) microscopy, 2D colloidal crystals etching, molten salt method, template method and hydrothermal/solvothermal method, [7-12] have been developed to synthesize various 2D nanostructures. Among the above mentioned methods, FIB is high cost, generally leading to the destruction of the crystal, such as the amorphous layers and formation of voids in some materials due to the use of high energy[13]. When molten salt method and template method are used, in order to obtain the pure products, a post-treatment is usually necessary to remove the template and impurities.[14-15]. Relatively, hydrothermal route is a convenient approach to realize the nanostructures. Moreover, a lot of hydrothermal conditions, such as thermal treatment temperature and time, solvents, minerallizers, modifiers, can be employed to influence the crystal nucleation and growth.

Perovskite-type $BiFeO_3$ (BFO) is one of the rare multiferroic compounds, in which ferroelectricity and magnetism coexist at room temperature. Despite of much effort on the BFO nanostructures for pursuing excellent multiferroic properties[16-21], as our acknowledgement, few reports are presented on the 2D single-crystal BFO nanostructure. Generally, the morphologies of crystalline particles depend on their crystal structure[22]. Under solution growth condition, an isotropic crystal structure of BFO basically leads to the cubic or spherical nanostructures without any surfactant. Therefore, it is difficult to obtain a 1D or 2D single-crystal BFO nanostructure by conventional solution growth. Nevertheless, it has been demonstrated that anisotropic nanostructures can be formed via self-assembly or selective adsorption through the introduction of surfactant in a chemical reaction[23,24]. In our previous researching work, the single-crystal tetragonal $PbZr_{0.52}Ti_{0.48}O_3$ (PZT) nanorods and nanowires have been realized by a polymer assisted hydrothermal route. The preferential adsorption of PVA and PAA on the (100) and (010) planes results in the PZT nanorods, and nanowires grow along the direction of [001][25]. Encouraged by previous work, we propose the use of appropriate raw material acting both as a reactant and a surface modifier to achieve the growth of 2D BFO microplates in a hydrothermal method.

Results and discussion

Fig. 1a shows the XRD patterns of the samples synthesized at 200 ºC for 12 h. All the diffraction peaks can be indexed to the rhombohedral $BiFeO_3$ (BFO) perovskite structure with the space group R3c (a_{hex}=b_{hex}=5.57874(16)Å, c_{hex}=13.8688(3) Å), agreeing well with the reported data by the standard card of JCPDS 86-1518. No peaks from other phases are detected, demonstrating that single-phase BFO powder has been successfully obtained under this condition. The strong and sharp diffraction peaks implies that the as-prepared BFO samples are well crystallized. Fig. 1b shows the SEM image of the

synthesized BFO samples. The as-prepared samples entirely consist of smooth microplates with about 8μm in lateral and about 510 nm in thickness (inset of Fig.1b). The BFO microplates were further characterized by HRTEM and SAED. Fig. 1d presents the HRTEM image of the BFO microplates. Three sets of fringe with intervals of 0.39 nm, 0.39 nm and 0.28 nm, which agree well with the spacing of (10-2), (1-12) and (2-10), respectively, are observed in the HRTEM image. Moreover, a corresponding SAED pattern along [241] zone axis (inset in Fig. 1d) is taken from one single BFO microplate by using the incident electron beam perpendicular to the BFO microplate. The SAED and HRTEM characterizations demonstrate the BFO microplates are single-crystal. Fig.1c presents the XRD patterns of the same powder samples which were cold pressed by the tablet machine. It is revealed that the intensity of the (012) and (024) diffraction peaks for BFO samples was strongly strengthened, while others strongly weakened, combining with the information given in the HRTEM image and SAED image (Fig. 1d), suggesting that the as-prepared single-crystal BFO microplates are dominated with (012) facets.

In order to understand the formation mechanism of the single-crystal BFO microplates, a series of time-dependent experiments were performed by changing the hydrothermal reaction time at 200ºC. The samples obtained at different stages of the hydrothermal reaction were characterized by XRD, SEM, TEM and SAED. Fig. 2 shows the XRD patterns of the samples obtained by hydrothermal treatment at 200 °C for different time of 6, 6.5, 7, 8 h. The XRD results reveal that at the initial stage the $Bi_{25}FeO_{40}$ phase firstly forms and then with the hydrothermal treatment time prolongation the $Bi_{25}FeO_{40}$ phase gradually disappears and transforms to pure rhombohedral BFO phase. When the hydrothermal reaction time is 6 h, the strong and sharp diffraction peaks can be indexed as $Bi_{25}FeO_{40}$ (JCPDS 46-0416) and a few weak diffraction peaks reflect the rhombohedral BFO phase (Fig. 2a), indicating at the initial stage the $Bi_{25}FeO_{40}$ phases firstly form. With the hydrothermal treatment time prolongation to 6.5 and 7 h, the diffraction peaks of $Bi_{25}FeO_{40}$ become very weaker, whiles BFO enhance strongly and sharply, implying that the firstly formed $Bi_{25}FeO_{40}$ phases gradually transforms to rhombohedral BFO phases. When the hydrothermal treatment time is prolonged to 8 h, because the transformation of $Bi_{25}FeO_{40}$ to BFO is complete, all the diffraction peaks can be well indexed to the rhombohedral perovskite [space group: R3c] phase of BFO (JCPDS 86-1518). No trace of other phase is observed in these XRD patterns.

Fig. 3 shows the SEM images of the hydrothermally synthesized samples at 200 ºC for different time of 6, 6.5, 7 and 8h, respectively. With the hydrothermal treatment time prolongation, the morphology of the obtained samples changes evidently. One can find that the samples obtained at 6 h, which is mainly composed of $Bi_{25}FeO_{40}$ phases, consist of nanoparticles (Fig. 3a). When the hydrothermal treatment time extend to 6.5 h, circle microplates, spherical nanoparticles and nanosheets are observed in the product, as shown in Fig. 3b. The circle microplates with size of 7μm possess a very rough surface. In addition, the inset of Fig. 3b (in the green rectangle) displays the circle microplate (thickness of 850nm) is self-assembled by a few pieces of nanosheets, the thickness of which is about 150nm. When the reaction time prolonged to 7h, only the circle microplates and nanosheets are obtained in the product. The spherical nanoparticles almost disappeared, as shown in Fig.3c. Noted that the surface of the circle microplates become relativity smooth compared to that of the circle microplates prepared at 6h. As the hydrothermal treatment time is prolonged to 8 h, rectangle shape microplates with relativity smooth surfaces (Fig. 3d) are obtained reflecting the formation of the pure rhombohedral BFO phases. The insets of Fig. 3(d) show the rectangle shape microplate with a side length of about 8μm and thickness of 550 nm. It should be emphasized that the thickness of microplates changed from 850nm (Fig.3b) to 510nm (Fig.1b) with the reaction time extension due to the surface reconstruction and Ostwald ripening process. On the basis of XRD and SEM results, we suggest that the formation of the microplates experienced the self-assembly, surface reconstruction and Ostwald ripening process.

Furthermore, we focused on the product prepared at 200 ºC for 6.5h. Fig.4 shows the microstructure of the sample characterized by TEM and HRTEM. Fig. 4a demonstrates the aggregation of the nanoparticles within 2D plan, implying that the nanosheet may be formed by 2D aggregation of nanoparticles. Fig. 4b shows the low-magnification TEM image of a nanosheet, beside which many nanoparticles were also observed. Fig. 4c is a HRTEM image of green rectangular area of Fig. 4b, where clear three-dimensional lattice stripes with interplanar spacing of 0.39nm, 0.39nm and 0.28nm, can be indexed into the (10-2), (1-12) and (2-10) of the rhombohedral structured BFO, respectively. The fast Fourier transform (FFT) pattern (Fig. 4d) of the corresponding HRTEM image displays regular diffraction spots, implying that the nanosheet is well-defined single crystal. Thus, it is proposed that the observed circle microplates (inset of Fig. 3b) with coarse surfaces are self-assembled by the single-crystal BFO nanosheets. According to the results in Fig. 4 and Fig. 2, this sample consists of both microplates and nanoparticles, which can be indexed into BFO and $Bi_{25}FeO_{40}$, respectively. The above results reveal that, the formation of BFO nanosheet experiences 2D aggregation of $Bi_{25}FeO_{40}$ nanoparticles. In addition, we suppose that organic ligands in the reaction system may play an important role in oriented-aggregation of $Bi_{25}FeO_{40}$ nanoparticles and self-assembly of BFO nanosheets.

To get further insight into the effect of precursor organic ligands on formation mechanism, FT-IR spectra of the products were studied, as shown in Fig. 5. Fig. 5a and 5b shows the FTIR spectra of raw materials ($C_6H_{10}BiNO_8$) and the BFO powder, respectively. And Fig .5c displays the FTIR spectra of the same powder dried at 100ºC for 24h, which eliminate the influence of the H_2O in the air. As shown in Fig.5b, the broad band at 3000-3600 cm^{-1} possibly arose from the antisymmetric and symmetric stretching of bond H_2O and OH^-, or from the symmetric stretching of bond N–H. The peaks located at 1628 cm^{-1} and 1385cm^{-1} can be assigned to the vibration of carbonyl groups and the symmetry bending vibration of C–H or C–H_2. The strong absorptive peak at 400-600 cm^{-1} is attributed to the Fe–O stretching and bending vibration, being characteristic of the octahedral FeO_6 groups in the perovskite compounds[26]. As observed in Fig. 5, two absorption bands such as those of C=O vibration (about 1600-1630 cm^{-1}) and N–H /O-H vibration (3000-

3500 cm^{-1}) both appear in the spectrum of the raw materials and products. These results indicate that organic ligands introduced by raw materials ($C_6H_{10}BiNO_8$) were possibly absorbed on the surface of product. It is suggested that the adsorption of the organic ligands on the nanoparticles play a key role in the 2D aggregation of nanoparticles and the subsequent formation of the microplates. In particular, these organic ligands, as a surface modifier, could selectively absorb on the (012) facets of the microplates, which leads to the formation of single-crystal BFO microplates with dominant (012) facets (as shown in Fig.1).

On the basis of the above discussion, we propose that the formation of the novel plate-like structure arises from a co-effect of 2D aggregate process, self-assemble process and Ostwald ripening. The whole process could be described by a simple model in Fig. 6. In the first stage, tiny nuclei are generated in the supersaturated solution and grown into $Bi_{25}FeO_{40}$ nanoparticles. In the second step, the spherical nanoparticles oriented-aggregation and grow within the 2D plan, resulting in the formation of the thin nanosheet. In this stage, detailed characterization of the sample (6.5h) showed the coexistence of small nanosheets and nanoparticles (Fig.4). As the mass diffusion and Ostwald ripening process proceed, thin nanosheets formed by consuming of the nanoparticles. Subsequently, the thin nanosheets self-assembled to microplates. The growth and self-assembly of small nanosheets was simultaneously occured, resulting in a coarse surface of the microplates. With the reaction time increasing, the uniform and smooth BFO microplates are formed by the surface reconstruction and Ostwald ripening process. In addition, another contribution to the formation of the microplates is organic ligand adsorption on the surface of $Bi_{25}FeO_{40}$ nanoparticles and BFO microplates. Specific manner of the adsorption may modify the formation mechanism by preventing contact between facets on which adsorption has occurred selectively[27]. The selective adsorption of these organic ligands may result in the formation of 2D structure and thus the microplate. Finally, as the growth proceeds, microplates are gradually formed by means of repeated dissolution-recrystallization process.

In order to explore the possible application of the BFO microplate, PVDF and BFO microplates were mixed and then made into composite film, the dielectric properties of the film was measured. Fig. 7 shows the frequency dependence of the dielectric permittivity (ε_r) and loss tangent ($\tan\delta$) of the BFO/PVDF thin film. Both the dielectric constant and dielectric loss decrease slowly with the frequency increase from 1000 Hz–1MHz. when the frequency increases above 1MHz, dielectric constant decrease sharply corresponding with the quickly increase of dielectric loss. It needs to be noted that the dielectric constant of BFO/PVDF film prepared by the present method is beyond 210 at 1MHz, which is much higher compared with those previously reported phase-pure BFO[28], BFO in ceramics[29-31] or films[32]. The dielectric constant is in the range of ε_r <130 for the BFO ceramics and in the range of ε_r <1~10 for the BFO film. For the dielectric loss, a resonance peak is observed at about 5MHz. The appearance of such resonance peak can be ascribed to the jumping of ions under external field[33]. The loss in this material generally originated from the higher conductivity causing higher leakage current[31]. The results indicated that the as-prepared BFO microplates show a promising for electronic device applications.

Experimental

The chemical reagents used in the work were ammonium bismuth citrate ($C_6H_{10}BiNO_8$), iron nitrate ($Fe(NO_3)_3{\cdot}9H_2O$), and potassium hydroxide (KOH). All the chemicals were analytical grade purity and were used as received without further purification.

In a typical procedure, $C_6H_{10}BiNO_7$ and $Fe(NO_3)_3{\cdot}9H_2O$ were dissolved in 20 ml distilled water in turn under continuous stirring. KOH solution was slowly added to the above solution to precipitate Fe^{3+} and Bi^{3+} ions under constant stirring to form a suspension. The obtained suspension was adjusted to 40 mL with distilled water and poured into the 50 ml homemade stainless-steel Teflon-lined autoclave and sealed for hydrothermal treatment. In the final suspension the KOH concentration was 0.4M. The hydrothermal reaction was performed by keeping the sealed autoclave in oven at 200 ^oC and kept for 12 h. After the hydrothermal treatment, the autoclave was pulled out the oven to cool down in air to room temperature. The products were filtered and washed with distilled water for several times, and then dried at 70 ^oC for 4 h, obtaining a brown powder.

The X-ray diffraction (XRD) patterns were measured on an ART-XRAY powder X-ray diffractmeter using the CuK□ (1.5418 Å) radiation with a scanning rate of 4 °/min. Scanning electron microscope (SEM) images were obtained from a SIRION field-emission scanning electron microscope (FEI, Eindhoven, the Netherlands). Transmission electron microscopy (TEM) images, selected area electron diffraction (SAED) patterns and high-resolution TEM (HRTEM) images were taken by a FEI F20 with an accelerating voltage of 200 kV. Fourier transforms infrared (FTIR) spectra of BFO powder was taken with a Nicolet Nexus 670 infrared spectrophotometer.

In order to prepare composite, poly-vinylidene fluoride (PVDF) was first dissolved in N, N-dimethylformamide (DMF) (Aldrich, 99.9%) obtaining transparent solution. Later, desired 30% (wt %) of previously prepared BFO powder were gradually added to this solution. The small amount of suspension was later transferred to spin coating machine's (KW-4A) chuck having glass slide to coat the suspension on the ITO glass. The spinning speed used was around 1600rpm. The coating progress was repeated two times and each process would take approximately 30 sec. The film was later kept in the oven at 90 °C to evaporate the remaining solvent. The final thickness of BFO/PVDF composite film was approximately 108.8 nm. Ag top electrodes of 2 mm*1 mm in diameter were sputtered as the top electrodes. Ag- BFO/PVDF-ITO parallel plate capacitances were formed to measure the dielectric properties by an impedance analyzer (Agilent 4294A) with an oscillating voltage of 50 mV at the frequency of 10 kHz.

Conclusions

In summary, we have developed a facile hydrothermal method to prepare single-crystal BFO microplates, where raw material ($C_6H_{10}BiNO_8$) acts both as a reactant and a surface modifier in the formation of BFO microplates. XRD, SEM, HRTEM results reveal that the microplates were dominated by (012) facets with

the lateral length of 8 μm and thickness of 510-550 μm. The formation of the BFO microplates possibly arise from a co-effect of 2D aggregate process, self-assemble process and Ostwald ripening. In addition, the dielectric constant of the BFO-PVDF film was determined to be ~210 in a frequency range from 1000 to 100 kHz, which is much higher than that pure BFO at room temperature. The facile synthesis approach and the proposed growth mechanism could provide new insights into the design and controlled synthesis of 2D materials. The acquisition of single-crystal 2D BFO will be beneficial not only for fundamental scientific research but also to providing good opportunity for device fabrications.

Acknowledgements

This work was financially supported by the National Natural Science Foundation of China (Grant no. 51232006, 51102212, 61274004).

Notes and references

[a] *Department of Materials Science and Engineering, Zhejiang University, Hangzhou 310027, P. R. China. Fax: 86-571-87952341; Tel: 86-571-87951649; E-mail:* msegxu@zju.edu.cn hgr@zju.edu.cn

† Electronic Supplementary Information (ESI) available: [details of any supplementary information available should be included here]. See DOI: 10.1039/b000000x/

‡ Footnotes

1. C. H. Ahn, K. M. Rabe and J. M. Triscone, *Science*, 2004, **303**, 488; N. A. Hill, *J. Phys. Chem. B*, 2000, **104**, 6694.
2. X. Wei, G. Xu, Z. Ren, C. Xu, G. Shen and G. Han, *J. Am. Ceram. Soc.*, 2008, **91**, 3795.
3. 3. J. J. Urban, W. S. Yun, Q. Gu and H. Park, *J. Am. Chem. Soc.*, 2002, **124**, 1186.
4. 4. Z. Ren, G. Xu, Y. Liu, X. Wei, Y. Zhu, X. Zhang, G. Lv, Y. Wang, Y. Zeng, P. Du, W. Weng, G. Shen, J. Z. Jiang and G. Han, *J. Am. Chem. Soc.*, 2010, **132**, 5572.
5. 5. X. Zhu, Z. Liu and N. Ming, *J. Mater. Chem.*, 2010, **20**, 4015-4030.
6. I. I. Naumov, L. Bellaiche and H. Fu, *Nature*, 2004, **432**, 737.
7. J. F. Scott, *Science*, 2007, **315**, 954; J. H. Zhang, Y. F. Li, X. M. Zhang and B. Yang, *Adv. Mater.*, 2010, **22**, 4249.
8. K. Yoon, D. Lee, H. Jung and S. Yoon, *J. Mater. Sci.*, 1992, **27**, 2941.
9. L. Ren, L. L. Ma, L. Jin, J. B. Wang, M. Q. Qiu and Y. Yu, *Nanotechnology*, 2009, **20**,405602.
10. Q. Feng, M. Hirasawa and K. Yanagisawa, *Chem. Mater.*, 2001, **13**, 290.
11. C. Chao, Z. Ren, Y. Zhu, Z. Xiao, Z. Liu, G. Xu, J. Mai, X. Li, G. Shen and G. Han, *Angew. Chem. Int. Ed.*, 2012, **51**, 9283.
12. J. Prado-Gonjal, M. E. Villafuerte-Castrejon, L. Fuentes and E. Moran, *Mater. Res. Bull.*, 2009, **44**, 1734.
13. M. Sugiyama and G. Sigesato, *J. Electron Microsc.*, 2004, **53**, 527.
14. M. Breysse, P. Afanasiev, C. Geantet and M. Vrinat, *Catal. Today*, 2003, **86**, 5.
15. M. Alexe, D. Hesse, V. Schmidt, S. Senz, H. J. Fan, M. Zacharias and U. Gösele, *Appl. Phys. Lett.*, 2006, **89**, 172907.
16. S. Dong, Y. Yao, Y. Hou, Y. Liu, Y. Tang and X. Li, *Nanotechnology*, 2011, **22**, 385701.
17. F. Gao, X. Y. Chen, K. B. Yin, S. Dong, Z. F. Ren, F. Yuan, T. Yu, Z. G. Zou and J. M. Liu, *Adv. Mater.*, 2007, **19**, 2889.
18. U. A. Joshi, J. S. Jang, P. H. Borse and J. S. Lee, *Appl. Phys. Lett.*, 2008, **92**,242106-1.
19. B. Liu, B. Hu and Z. Du, *Chem. Commun.*, 2011, **47**, 8166.
20. S. H. Xie, J. Y. Li, R. Proksch, Y. M. Liu, Y. C. Zhou, Y. Y. Liu, Y. Ou, L. N. Lan and Y. Qiao, *Appl. Phys. Lett.*, 2008, **93**, 222904-1.
21. L. W. Martin, *Dalton T.*, 2010, **39**, 10813.
22. I. Pribosic, D. Makovec and M. Drofenik, *Chem. Mater.*, 2005, **17**, 2953.
23. Z. Ren, G. Xu, X. Wei, Z. Liu, Y. Wang, Z. Xiao, G. Shen and G. Han, *J. Cryst. Growth*, 2009, **311**, 4593.
24. Z. Liu, Z. Ren, Z. Xiao, C. Chao, X. Wei, Y. Liu, X. Li, G. Xu, G. Shen and G. Han, *Small*, 2012, **8**, 2959.
25. G. Xu, Z. H. Ren, P. Y. Du, W. J. Weng, G. Shen and G. R. Han, *Adv. Mater.*, 2005, **17**, 907.
26. G. V. S. Rao, C. N. R. Rao and J. R. Ferraro, *Appl. Spectrosc.*, 1970, **24**, 436.
27. J. Polleux, N. Pinna, M. Antonietti and M. Niederberger, Adv. Mater., 2004, **16**, 436.
28. A. Gajovic, S. Sturm, B. Jancar, A. Santic, K. Zagar and M. Ceh, *J. Am. Ceram. Soc.*, 2010, **93**, 3173.
29. G. L. Yuan, S. W. Or, Y. P. Wang, Z. G. Liu and J. M. Liu, *Solid State Commun.*, 2006, **138**, 76.
30. J. K. Kim, S. S. Kim and W.-J. Kim, *Mater. Lett.*, 2005, **59**, 4006.
31. A. K. Pradhan, K. Zhang, D. Hunter, J. B. Dadson, G. B. Loiutts, P. Bhattacharya, R. Katiyar, J. Zhang, D. J. Sellmyer, U. N. Roy, Y. Cui and A. Burger, *J. Appl. Phys.*, 2005, **97**, 093903.
32. V. R. Palkar, J. John and R. Pinto, *Appl. Phys. Lett.*, 2002, **80**, 1628.
33. J. Chen, X. Xing, A. Watson, W. Wang, R. Yu, J. Deng, L. Yan, C. Sun and X. Chen, *Chem. Mater.*, 2007, **19**, 3598.

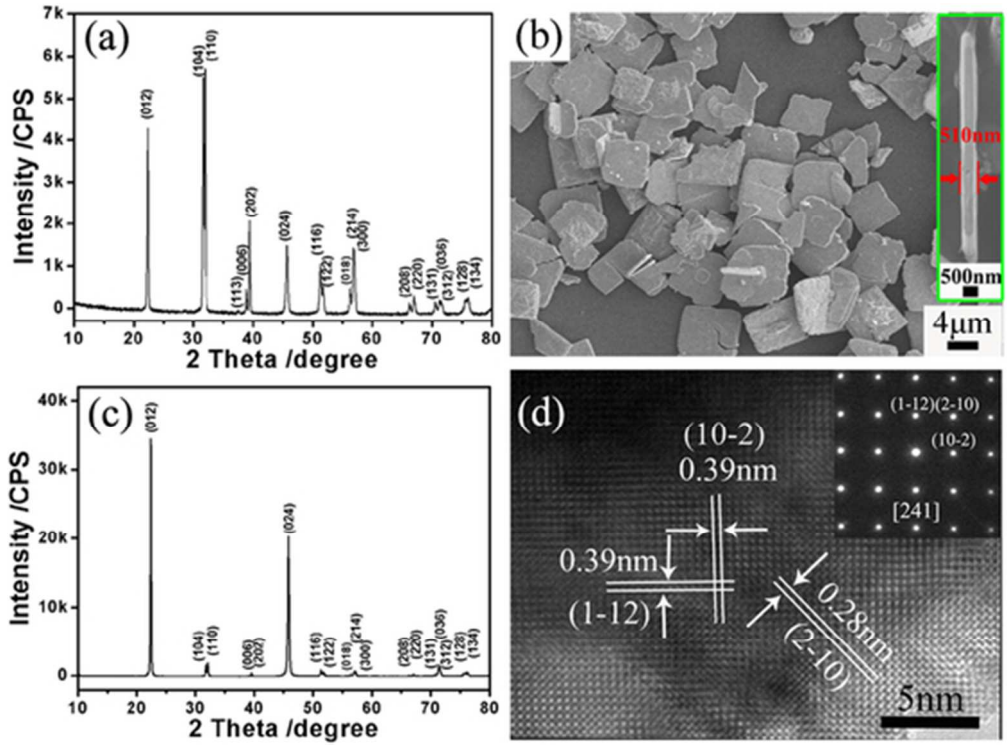

Fig. 1(a) XRD pattern of the as-prepared BFO microplates hydrothermally treated for 12h, (b) Low magnification and magnified (inset) SEM images of the samples, (c) XRD pattern of the same sample which was pressed compaction, (d) HR-TEM image of the BFO microplates, the inset is the SAED pattern.
23x17mm (600 x 600 DPI)

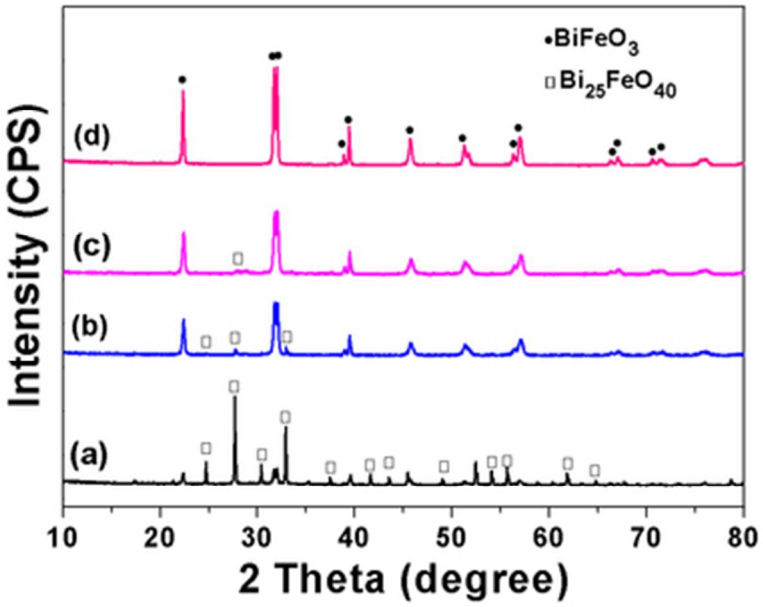

Fig. 2 XRD patterns of the as-prepared BFO products hydrothermally treated for different time. (a) 6h, (b) 6.5h, (c) 7h and (d) 8h.
16x13mm (600 x 600 DPI)

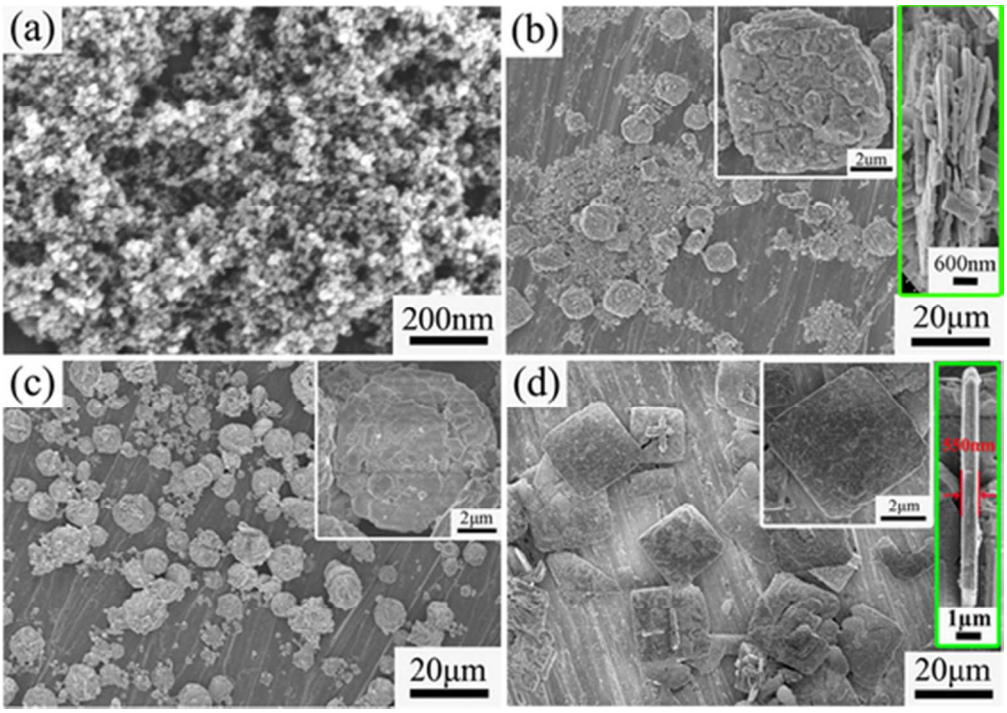

Fig. 3 SEM images of the samples hydrothermal treatment for different time. (a) 6 h, (b) 6.5 h, (c) 7 h and (d) 8 h.
22x15mm (600 x 600 DPI)

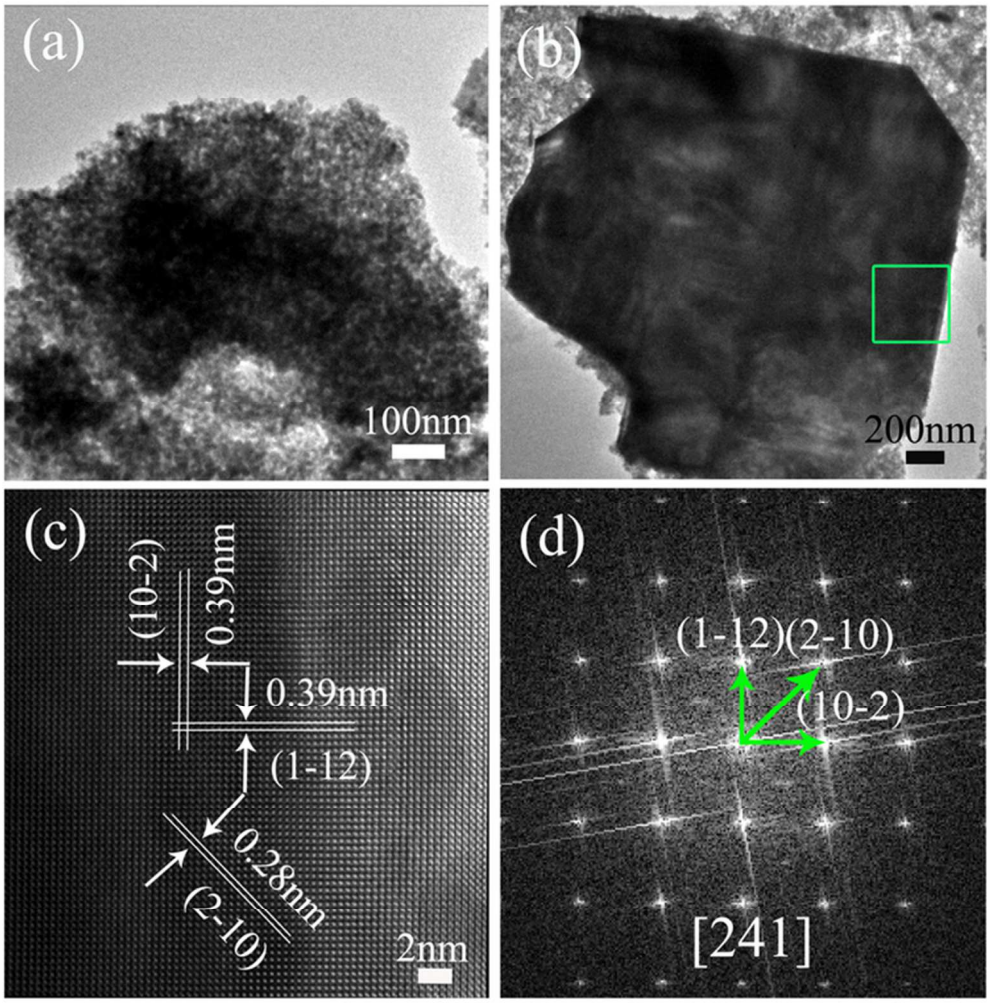

Fig. 4(a) TEM images of the nanoparticles synthesized hydrothermally at 200℃ for 6.5h. (b) TEM images of the nanoplate synthesized hydrothermally at 200℃ for 6.5h. (c) The corresponding HRTEM images of the green rectangular area in (b). (d) shows the corresponding fast Fourier transform(FFT) ED pattern of (c)(indexed as the[241] zone axis).
32x32mm (600 x 600 DPI)

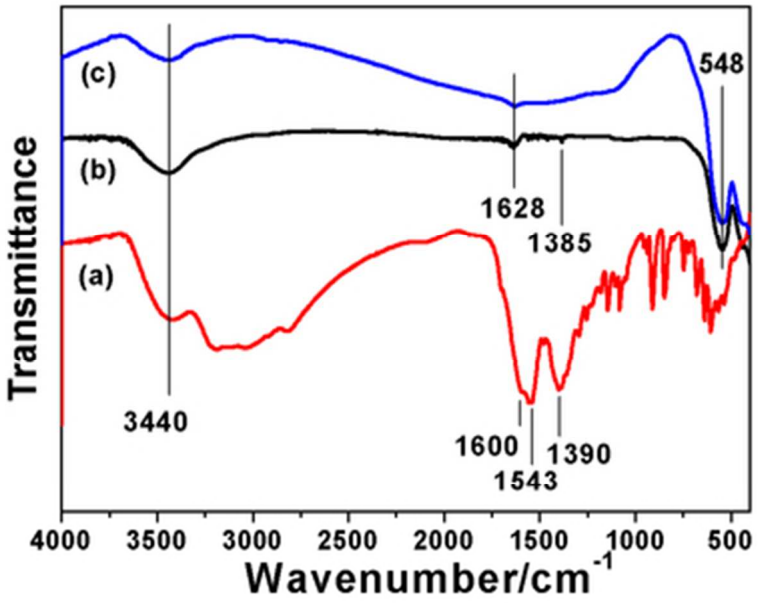

Fig. 5 (a) FT-IR spectra of ammonium bismuth citrate (C6H10BiNO8) (b) FT-IR spectra of BFO powder hydrothermal synthesized for 12h (c) FT-IR spectra of the same BFO sample dried at 100℃ for 24h.
16x13mm (600 x 600 DPI)

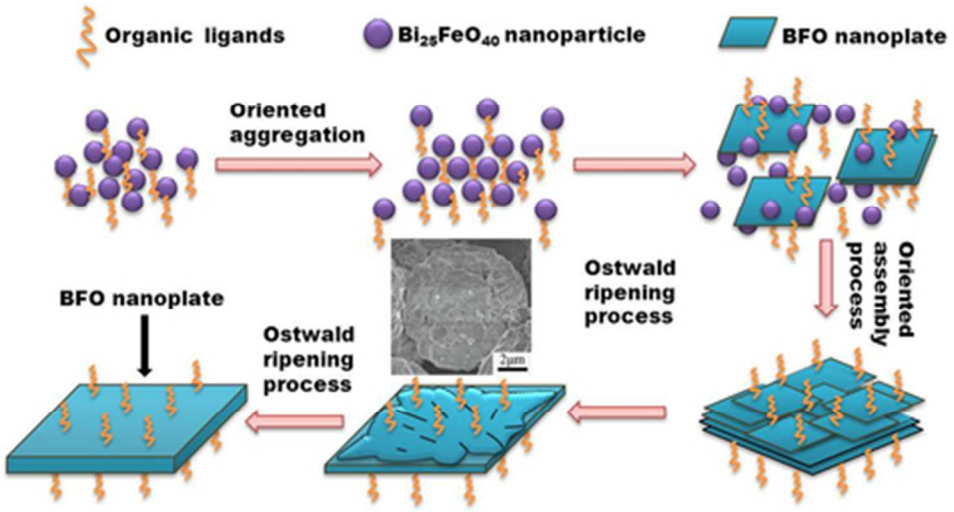

Fig. 6 Formation and shape-evolution process of BFO microplates.
20x10mm (600 x 600 DPI)

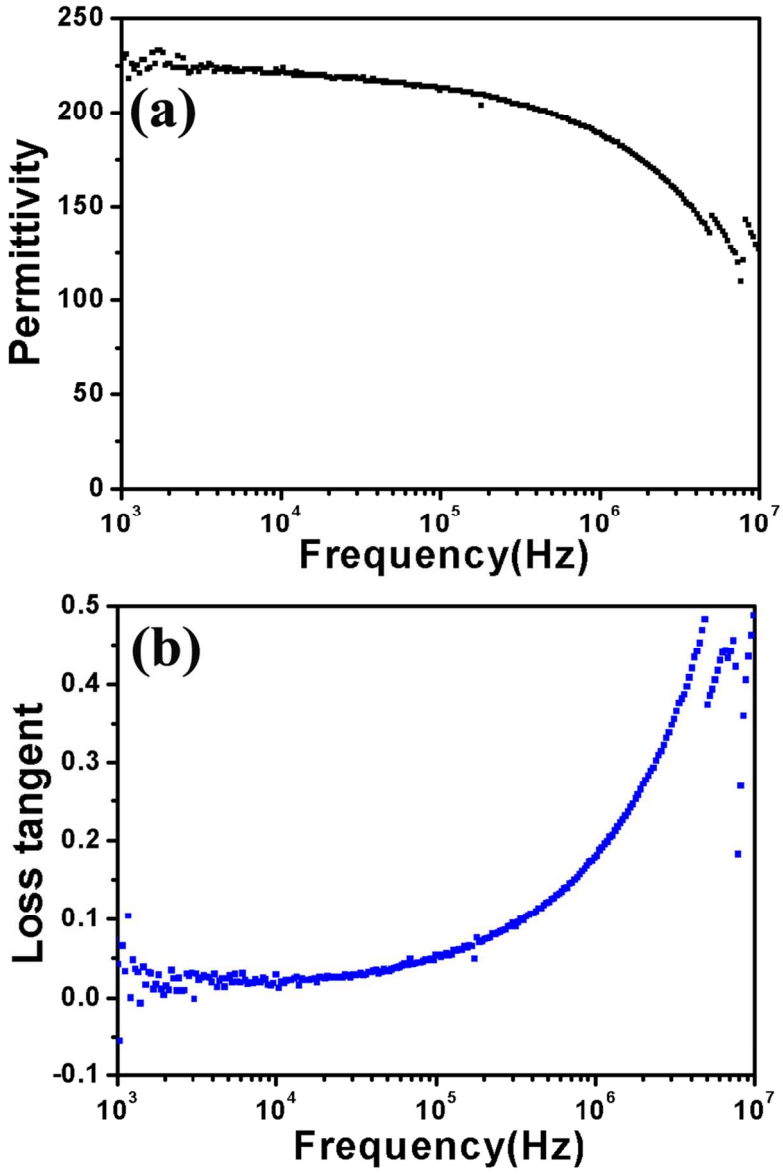

Fig.7 Dielectric behaviors of BFO-PVDF thin films.
48x75mm (600 x 600 DPI)

Figure caption

Fig. 1(a) XRD pattern of the as-prepared BFO microplates hydrothermally treated for 12h, (b) Low magnification and magnified (inset) SEM images of the samples, (c) XRD pattern of the same sample which was pressed compaction, (d) HR-TEM image of the BFO microplates, the inset is the SAED pattern.

Fig. 2 XRD patterns of the as-prepared BFO products hydrothermally treated for different time. (a) 6h, (b) 6.5h, (c) 7h and (d) 8h.

Fig. 3 SEM images of the samples hydrothermal treatment for different time. (a) 6 h, (b) 6.5 h, (c) 7 h and (d) 8 h.

Fig. 4(a) TEM images of the nanoparticles synthesized hydrothermally at 200℃ for 6.5h. (b) TEM images of the nanoplate synthesized hydrothermally at 200℃ for 6.5h. (c) The corresponding HRTEM images of the green rectangular area in (b). (d) shows the corresponding fast Fourier transform(FFT) ED pattern of (c)(indexed as the[241] zone axis).

Fig. 5 (a) FT-IR spectra of ammonium bismuth citrate ($C_6H_{10}BiNO_8$) (b) FT-IR spectra of BFO powder hydrothermal synthesized for 12h (c) FT-IR spectra of the same BFO sample dried at 100℃ for 24h.

Fig. 6 Formation and shape-evolution process of BFO microplates.

Fig.7 Dielectric behaviors of BFO-PVDF thin films.

Graphical abstract

Single-crystal $BiFeO_3$ (BFO) microplates with dominant (012) facets were successfully synthesized by a facile one-pot hydrothermal method without any polymer additives. The results of XRD, SEM, TEM and FT-IR indicate that adsorption behaviour of the organic ligands could play key role in the formation of the BFO microplates.